Organ-Specific and Size-Dependent Ag Nanoparticle Toxicity in Gills and Intestines of Adult Zebrafish

Olivia J. Osborne,[†,§] Sijie Lin,[†,§] Chong Hyun Chang,[†] Zhaoxia Ji,[†] Xuechen Yu,[†] Xiang Wang,[†] Shuo Lin,[‡] Tian Xia,[†,⊥] and André E. Nel*[,†,⊥]

[†]Center for Environmental Implications of Nanotechnology, California NanoSystems Institute, University of California, Los Angeles, Los Angeles, California 90095, United States, [‡]Department of Molecular, Cell, and Developmental Biology, University of California, Los Angeles, Los Angeles, California 90095, United States, and [⊥]Department of Medicine, Division of NanoMedicine, UCLA School of Medicine, 52-175 CHS, 10833 Le Conte Ave, Los Angeles, California 90095, United States. [§]Olivia Osborne and Sijie Lin contributed equally.

ABSTRACT We studied adult zebrafish to determine whether the size of 20 and 110 nm citrate-coated silver nanoparticles (AgC NPs) differentially impact the gills and intestines, known target organs for Ag toxicity in fish. Following exposure for 4 h, 4 days, or 4 days plus a 7 day depuration period, we obtained different toxicokinetic profiles for different particle sizes, as determined by Ag content of the tissues. Ionic $AgNO_3$ served as a positive control. The gills showed a significantly higher Ag content for the 20 nm particles at 4 h and 4 days than the 110 nm particles, while the values were more similar in the intestines. Both particle types were retained in the intestines even after depuration. These toxicokinetics were accompanied by striking size-dependent differences in the ultrastructural features and histopathology in the target organs in response to the particulates. Ag staining of the gills and intestines confirmed prominent Ag deposition in the basolateral membranes for the 20 nm but not for the 110 nm particles. Furthermore, it was possible to link the site of tissue deposition to disruption of the Na^+/K^+ ion channel, which is also localized to the basolateral membrane. This was confirmed by a reduction in ATPase activity and immunohistochemical detection of the α subunit of this channel in both target organs, with the 20 nm particles causing significantly higher inhibition and disruption than the larger size particles or $AgNO_3$. These results demonstrate the importance of particle size in determining the hazardous impact of AgNPs in the gills and intestines of adult zebrafish.

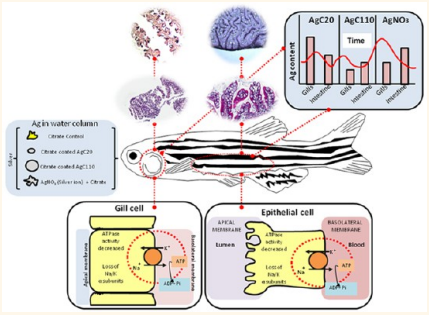

KEYWORDS: Ag nanoparticles · size dependent · toxicokinetics · histopathology · Na^+/K^+ ATPase pump · zebrafish

As the nanotechnology industry continues to expand, so does nanoparticle (NP) production, with over 2000 nanoproducts currently in the marketplace.[1] As a result of their attractive antimicrobial properties, silver nanoparticles (AgNPs) are one of the most abundant commercially available nanomaterials, with over 400 nanoproducts containing nano-Ag.[2,3] AgNPs are found in many consumer products (See Table S1) such as cosmetics, plastics, water purifiers, textiles, medicine, and every day applications.[4] Consequently, this amplifies the likelihood of AgNPs reaching water systems, with the possibility of exposing aquatic organisms that reside there. Research using life cycle modeling predicts that the amount of AgNPs reaching surface waters may amount to >60 tons per year,[5] with the possibility of causing hazardous effects in aquatic life forms such as fish and fish embryos.[6]

Although Ag toxicity in aquatic organisms,[7] with an emphasis on fish,[8] has been discussed since the 1930s,[9] consideration of nano-Ag toxicity has emerged more recently with the advent of nanotechnology. This raises the interesting question about the contribution of the physicochemical properties of AgNPs, over and above the importance of the released Ag ions, on aquatic species such as algae,[10] daphnia,[11] zebrafish embryos,[12] and adult fish. For instance, AgNPs cause respiratory stress[13] in adult Eurasian perch and oxygen radical production in the livers of adult zebrafish.[14] In addition, research has been launched into the mechanism(s) of AgNP toxicity *in vivo* and *in vitro*.[15,16] While most of these studies have considered comparison of particulate with ionic toxicity,[17] not much consideration was given to how specific NP physicochemical characteristics, such as size, impact toxicological outcome.

* Address correspondence to anel@mednet.ucla.edu.

Received for review July 23, 2015 and accepted September 1, 2015.

Published online September 01, 2015
10.1021/acsnano.5b04583

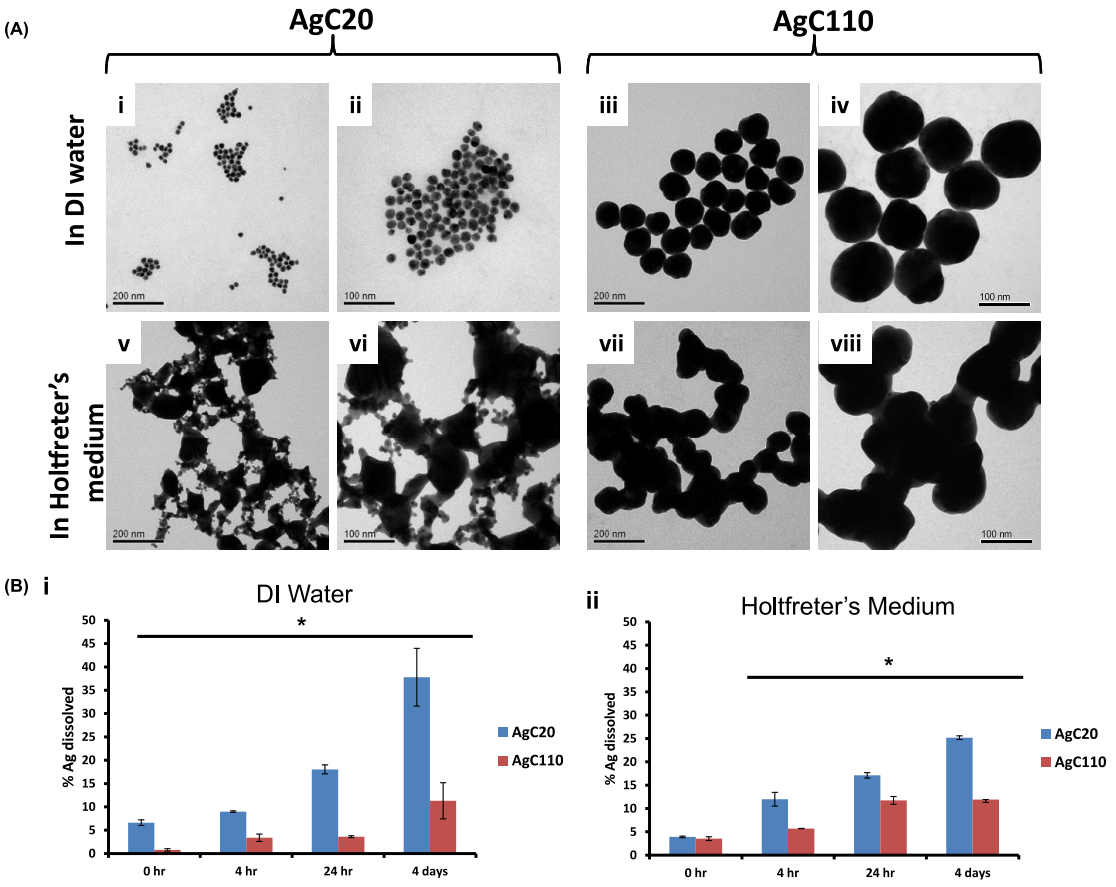

Figure 1. Physicochemical characterization and dissolution characteristics of the nanoparticles. (A) Representative TEM images of AgC20 and AgC110 in DI and Holtfreter's medium (HM) to show the primary size, shape, and state of agglomeration of the particles. (i) AgC20 particles in DI water at 150000 magnification; (ii) AgC20 particles in DI water at 300000 magnification; (iii) AgC110 particles in DI water at 150000 magnification; (iv) AgC110 in DI water at 300000 magnification; (v) AgC20 particles in HM at 150000 magnification; (vi) AgC20 particles in HM at 300000 magnification; (vii) AgC110 particles in HM at 150000 magnification; (viii) AgC110 in HM at 300000 magnification. (B). Dissolution characteristics in DI water and HM. (i) Dissolution of AgC20 and AgC110 particles in DI water at t = 0, 4 h, 24 h, and 4 days. (ii) AgC20 and AgC110 dissolution in HM for the same time periods. AgC20 particles had a significantly (*p < 0.05) higher dissolution rate than AgC110 particles in both dissolution media.

However, we have previously demonstrated that smaller AgNPs exert more hazardous effects in zebrafish embryos than larger particles.[18] It is also known that 20 nm AgNPs induce more intense inflammation and oxidative stress in the lungs of rodents than 110 nm particles, as a result of the increased rate of dissolution of the smaller particles.[19] Knowing this, we were interested to determine whether different particle sizes could impact known target organs for hazardous substances in fish, namely, the gills and intestines.[20,21] In addition, we wanted to know whether size-dependent variances are differently reflected in the target organs, as well as known mechanistic targets for Ag^+ in the fish gill, including the ionoregulatory Na^+/K^+ ATPase pump[22] (Figure S4).

Against this background, we set out to perform a comprehensive analysis of the effect of 20 versus 110 nm citrate-coated AgNPs in adult zebrafish, utilizing a wide range of end points to assess the toxicokinetics, organ pathology, tissue-specific Ag deposition, and impact on the Na^+/K^+ ATPase channel. We also compared the particle effects to an ionic control ($AgNO_3$), which has previously been shown to exert toxicity in adult zebrafish.[23] Our data demonstrate differences in the toxicokinetics of particulate versus ionic Ag, as well as size-dependent differences that reflect the higher bioavailability and toxicological impact of smaller particles compared with larger particles.

RESULTS

Physicochemical Characterizations of the AgNPs. To investigate the hazard potential of AgNPs, two citrate-coated AgNPs with primary sizes 20 and 110 nm (AgC20 and AgC110) were purchased from nanoComposix (San Diego, CA). The primary particle sizes and shapes were characterized by transmission electron microscopy (TEM), while ZetaPALS was used to assess hydrodynamic sizes and surface charge (ζ-potential) in DI water or Holtfreter's medium (HM) (Figure 1A and Table 1). While the hydrodynamic sizes in DI water were 25.01 $\pm$ 0.1 and 73.1 $\pm$ 0.8 for AgC20 and AgC110, respectively, particle agglomeration in HM resulted in

TABLE 1. NP Hydrodynamic Diameter and ζ-Potential in DI Water and Holtfreter's Medium

	DI water			HM		
NPs	d_H (nm)	PDI[a]	ζ-potential (mV)	d_H (nm)	PDI[a]	ζ-potential (mV)
AgC20	25.01 ± 0.1	0.053	−9.3 ± 1.5	522.2 ± 37.3	0.323	−16.6 ± 2.1
AgC110	73.1 ± 0.8	0.278	−25.4 ± 4.8	340.5 ± 9.7	0.257	−23.7 ± 2.6

[a] Polydispersity index.

Scheme 1. Schematic To Show the Experimental Layout[a]

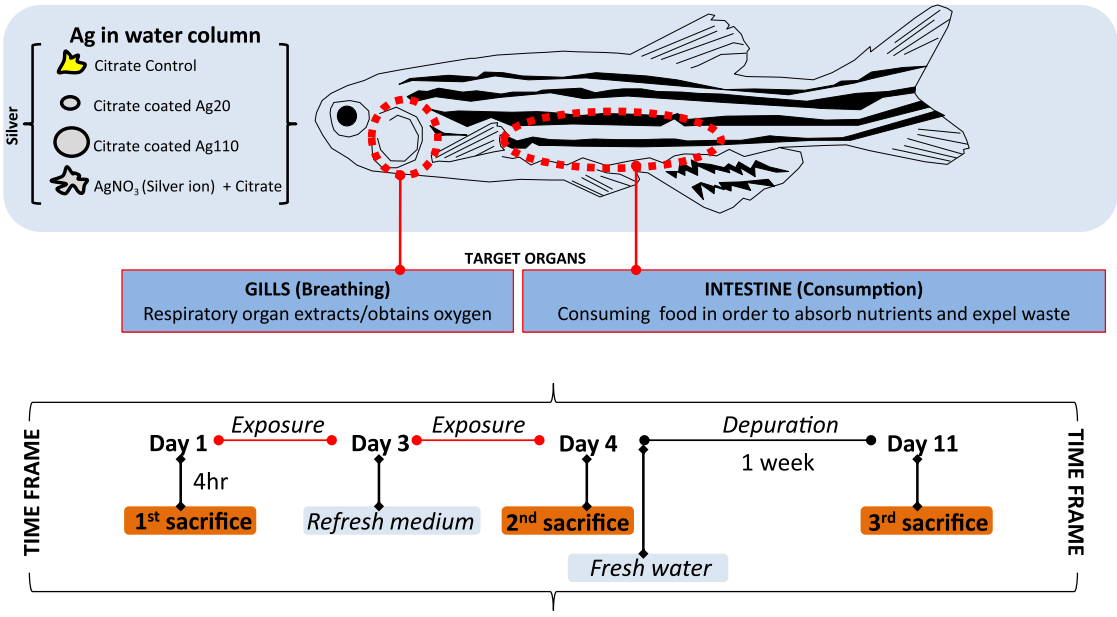

[a] There were four treatment groups: control + citrate, citrate-coated 20 nm Ag (AgC20), citrate-coated 110 nm Ag (AgC110) and ionic Ag ($AgNO_3$) with added citrate. Zebrafish exposure commenced on day 1, at a [Ag] of 1 ppm. One group of animals exposed for 4 days underwent an additional week of depuration by transferring zebrafish into a clean medium. Fish were sacrificed at 3 time points as shown, namely, exposure for 4 h or 4 days, as well as on day 11 (*i.e.*, 4 days of exposure + 7 days depuration).

increased hydrodynamic sizes of 552.2 ± 37.3 and 340.5 ± 9.7 nm, respectively (Table 1). This size change was also confirmed in the representative TEM images (Figure 1A,v−viii). AgC110 particles had a ζ-potential of −25.4 ± 4.8 in DI and −23.7 ± 2.6 in HM, while the corresponding values for AgC20 were −9.6 ± 1.5 in DI water and −16.6 ± 2.1 in HM, respectively (Table 1).

Because particle dissolution plays a critical role in AgNP toxicity in aquatic systems, we also determined particle dissolution rates in DI water and HM using inductively coupled plasma optical emission spectroscopy (ICP-OES). Both particles showed exponential increases in Ag shedding in DI water and HM following incubation for 4 h, 24 h, and 4 days (Figure 1B,i,ii). The AgC20 particles showed a significantly ($p < 0.05$) higher dissolution rate than the AgC110 particles in both media (Figure 1B,ii).

Quantification of the Ag Content of the Gills and Intestines Reveals Size-Dependent Differences. ICP-OES analysis was used to assess the toxicokinetic profiles of AgC20, AgC110, and $AgNO_3$ following the exposure of adult zebrafish as shown in Scheme 1. Briefly, the animals were exposed to the different Ag treatments for 4 h (day 1), 4 days (day 4), or 4 days plus a depuration period of 7 days in fresh HM (*i.e.*, day 11). Quantification of the total Ag content of the gills and intestines at sacrifice (days 1, 4 and 11; Scheme 1), demonstrated discernible Ag uptake in the gills and intestines (Figure 2A), with little or no Ag present in the brain, liver, and gonads (data not shown). As shown in Figure 2A, there were significant differences ($p < 0.05$) between the gills of unexposed versus particulate treated fish after 4 h and 4 days. Particularly noticeable at 4 h is the significantly ($p < 0.05$) higher Ag content for 20 nm particles compared with either AgC110 or $AgNO_3$ in the gills. These size dependent Ag uptake differences were maintained at 4 days, with AgC20 showing 3-fold higher Ag uptake than AgC110 or $AgNO_3$ (*i.e.*, AgC20 > $AgNO_3$ > AgC110). Interestingly, after a 7-day depuration period, there was low or no detectable Ag retention in the particulate exposed animals, with a trace of Ag showing in the gills of fish exposed to the ionic form.

Similar but less dramatic differences were seen between the control and the Ag treatment groups

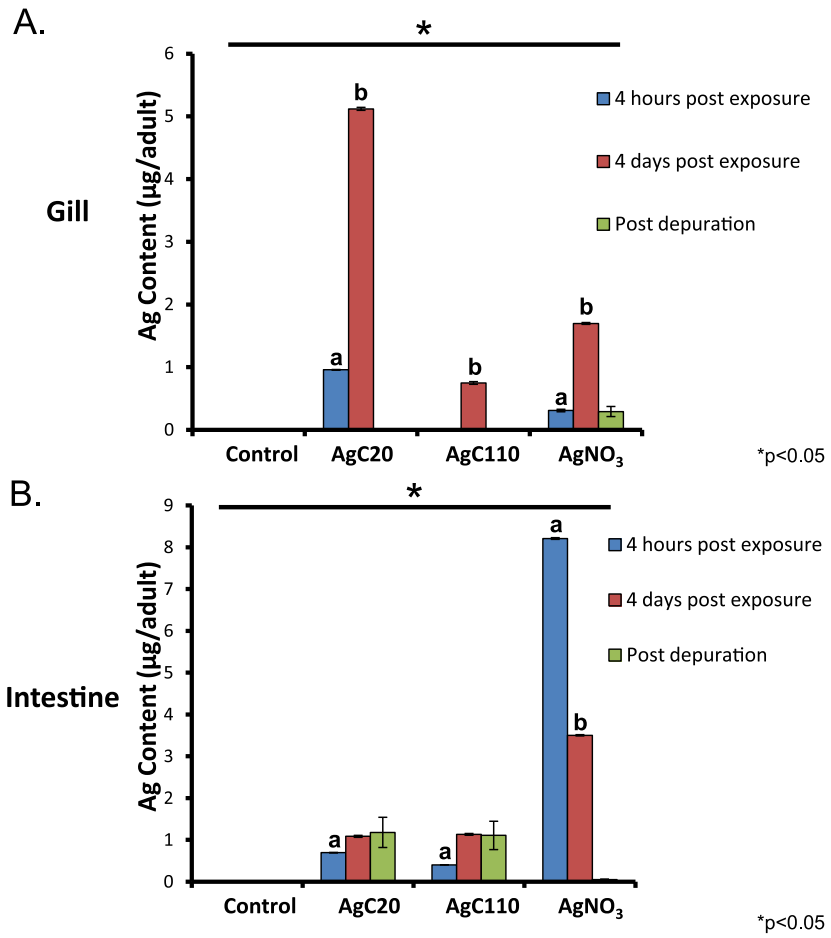

Figure 2. Toxicokinetic profiles of AgC20 and AgC110 in gills and intestines at 4 h postexposure (4hpe) (blue bars), 4 days postexposure (4dpe) (red bars), and 4 days + 7 days depuration (green bars). The total amount of Ag per adult zebrafish was determined by ICP-OES measurement. (A) Graph showing the amount of Ag (in μg) in the gills per adult fish (expressed as μg/fish). There were significant differences ($p < 0.005$) between control and Ag-exposed animal groups, as shown by a line plus an asterisk between groups being compared. There were also statistically significant ($p < 0.05$) differences between AgC20, AgC110, and $AgNO_3$ at 4hpe (marked with the letter a), and at 4dpe (marked with the letter b) (B) Graph showing the amount of Ag in the intestine of exposed animals. There were overall significant differences ($p < 0.005$) between control and treatment groups, as indicated by a line and an asterisk. There were significant differences between treatment groups at 4 hpe (marked with the letter a) and 4 dpe (marked with the letter b). Please notice that the nanoparticulate groups had significantly higher amounts of Ag accumulating on day 11 (post-depuration) compared with the ionic form ($p < 0.05$).

during analysis of intestinal tissue (Figure 2B). At 4 h post exposure, $AgNO_3$ resulted in a significantly ($p < 0.05$) higher Ag content compared with AgC20 or AgC110 exposures. This trend was also observed at 4 days postexposure. Although not as obvious as in the gills, AgC20 exposure was responsible for a significantly higher ($p < 0.05$) Ag content than AgC110 at 4 h. However, $AgNO_3$ exposure led to significantly ($p < 0.05$) higher Ag uptake than either of the particulates at 4 h and day 4. This was not true though for Ag retention after depuration, where a much greater amount of Ag was detected in the intestines for animals exposed to the particulates vs the ionic form (Figure 2B).

Histopathological Features of Gill and Intestine by Nano-Ag and Ionic-Ag. In order to perform histopathological analysis of the gills and intestines in response to the various exposures, samples were collected at the time of the second sacrifice (day 4, Scheme 1) for paraformaldehyde (PFA) fixation, sectioning, H&E staining and histological analysis. The histology of a normal gill in nonexposed fish is shown in Figure 3A,i. This demonstrates intact primary and secondary filaments (further illustrated by the idealized diagram in Figure S2A) without noticeable damage, including the presence of erythrocytes, basal cells, and an intact cytoskeleton. In contrast, low magnification viewing demonstrated clearly observable morphological changes in the gills of fish exposed to nano-Ag and $AgNO_3$, with the more striking impact in fish exposed to ionic Ag (Figure 3A,i,ii); this is in agreement with previous observations.[23] Lower magnification images (Figure 3A,iii) of the gill tissue collected from AgC20 exposed zebrafish demonstrated the loss of distinguishable primary and secondary filaments, as a result of fusion of the secondary filaments. Higher magnification viewing of the same sections demonstrates prominent hyperplasia and inflammation, accompanied

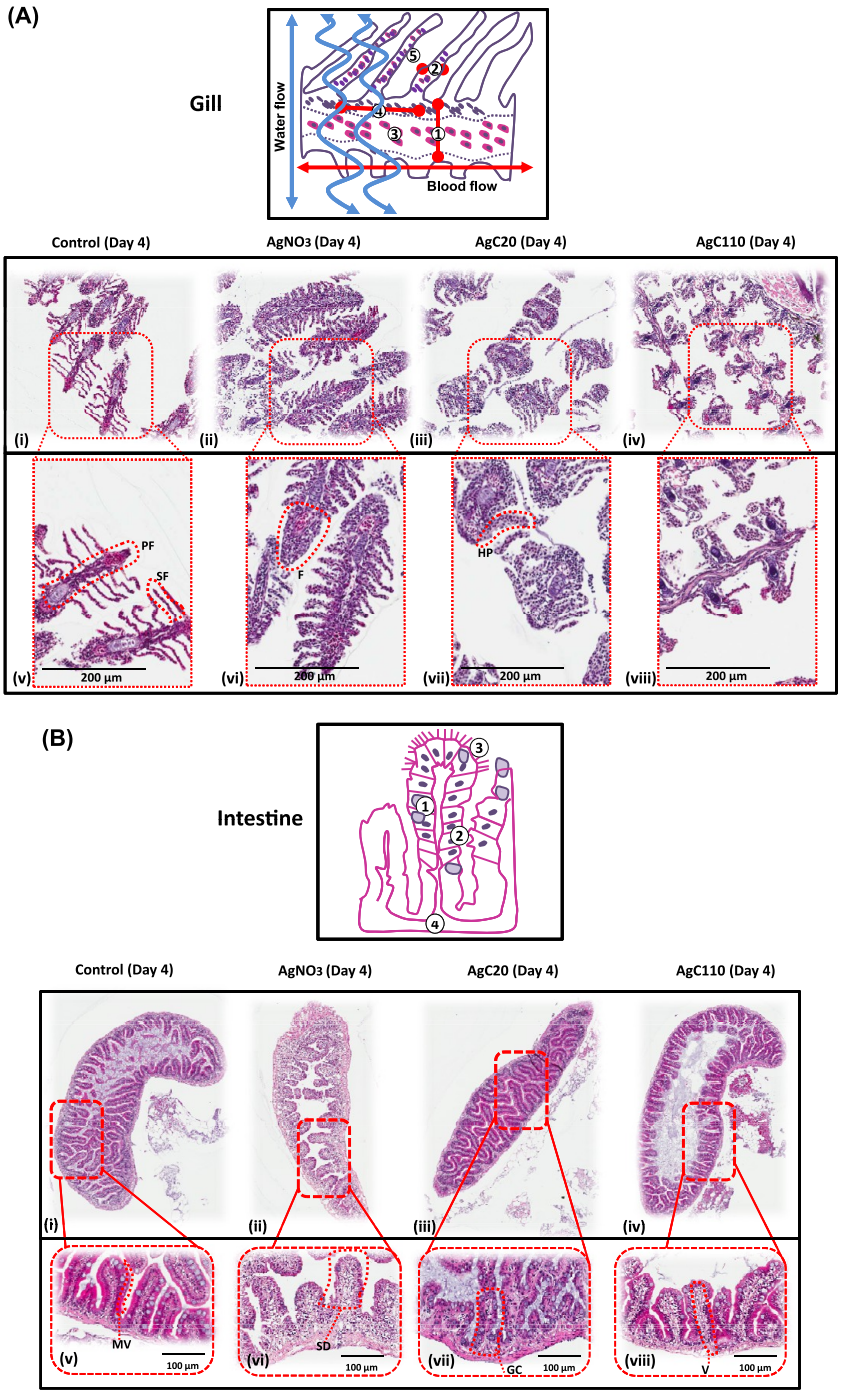

Figure 3. Representative histological images of gill and intestinal tissues. (A) Idealized diagram (top) depicting the key features of a normal gill: (1) primary filament; (2) secondary filament; (3) erythrocyte; (4) basal cells; (5) mucous cells. Gill tissue (bottom). (i−iv) Low magnification (10×) images of zebrafish gills: (i) normal histology in nonexposed animals; (ii) $AgNO_3$ treated fish, displaying prominent damage, including fusion of secondary filaments; (iii) AgC20 treated fish, displaying severe hyperplasia and fusion of secondary filaments; (iv) AgC110 treated fish, displaying hyperplasia and fusion that is not as prominent as for AgC20. (v−viii) Gill tissue 20× images: (v) normal gill histology, with highlighting of primary (PF) and secondary filaments (SF); (vi) $AgNO_3$ treated fish, with fusion as marked by F; (vii) AgC20 treated fish, with the highlighted area showing severe hyperplasia (HP) in secondary filaments; (viii) AgC110 treated fish showing less fusion/hyperplasia compared with AgC20. (B) Idealized diagram (top) illustrating the key features of a normal intestine: (1) goblet cells; (2) enterocytes; (3) microvilli; (4) basolateral membrane. Intestinal tissue (bottom). (i−iv) Low magnification (4×) images: (i) normal intestinal tissue; (ii) $AgNO_3$-treated fish, showing extensive structural damage, vacuolization, and nearly complete loss of microvilli; (iii) AgC20-treated fish, showing goblet cell hyperplasia, vacuolization, and partial loss of microvilli; (iv) AgC110-treated fish, showing some vacuolization but intact microvilli. (v−-viii) Intestinal tissue, 10× images: (v) Normal intestinal tissue, with the dotted red line showing microvilli (MV); (vi) $AgNO_3$ treated fish, with the red line highlighting structural destruction (SD); (vii) AgC20-treated fish with the red line outlining goblet cells (GC); (viii) AgC110-treated fish with the red line outlining vacuolization (V).

by a decreased number of erythrocytes and the appearance of clusters of mucoid cells on the secondary filaments (Figure 3A,vii). In contrast, the gill structure of AgC110 exposed fish demonstrated less prominent changes with better preservation of the primary and secondary filament structure (Figure 3A,iv,viii). Nonetheless, the secondary filaments exhibited some hyperplasia and the presence of erythrocytes. However, compared with the particulates, the most prominent evidence of inflammation and fusion of the secondary filaments were seen in the fish exposed to $AgNO_3$ (Figure 3A,ii,vi).

The intestinal histology of a normal, nonexposed fish is shown in Figure 3B,i. This demonstrates the presence of an intact gut lumen and microvilli covered by an epithelial layer (with goblet cells), which overlays the lamina propria, muscularis externa, and serosa (see the idealized diagram explaining the features of a normal intestine in Figure S3A). Low magnification images demonstrated that $AgNO_3$ treatment (Figure 3B,ii), as in the gills, was responsible for the most striking morphological changes. These included almost complete obliteration of the lamina propria, as a result of inflammatory infiltrates, epithelial vacuolization, and loss of microvilli, as demonstrated in the higher magnification views (Figure 3B,vi). The intestinal structure was better preserved in the AgC20 treatment group (Figure 3B,iii), which showed an increased number of goblet cells in the epithelial layer, some reduction in microvilli, and partial damage to the lamina propria (Figure 3B,vii). In contrast, the AgC110 treated group showed evidence of vacuolization and partial lamina propria damage with abundant microvilli (Figure 3B,viii).

Ag Staining of Gill Tissue Reveals Differences in the Localization of Particulate vs Ionic Ag. In order to see whether the histopathological differences correlate with the site of Ag deposition, Ag staining[19] was used to examine the same gill and intestinal tissue sections used for Figure 3A,B. This demonstrated that nano-Ag (Figure 4A,iii,iv) adhere to the secondary filaments (Figure S2A), particularly AgC20 particles (Figure 4A,iii,v), which is in agreement with the high Ag content in the gills on day 4 (Figure 2A). In comparison, $AgNO_3$ treatment (Figure 4A,ii) demonstrated the presence of Ag mostly in the primary filaments (Figure S2A) with little or no staining of the secondary filaments. In conclusion, the nanoparticulate Ag primarily deposits in secondary filaments, while the ionic Ag is primarily retained in primary filaments.

Ag Staining of Intestinal Tissue Reveals Differences in the Localization of Particulate vs Ionic Ag. Use of the same Ag staining method demonstrated that the most prominent staining occurred in the basolateral membrane of the intestinal mucosa during AgC20 exposure (Figure 4B,iii; Figure S3). The same effect was not seen during AgC110 treatment (Figure 4B,iv) or exposure to $AgNO_3$ (Figure 4B,ii), suggesting that the relatively small size of the 20 nm Ag particles is responsible for compartmentalized deposition in the intestines. The same effects were not seen in fish exposed to 110 nm particles, with most of the Ag staining occurring on the apical membrane of the intestinal epithelial cells (Figure 4B,iv). Most staining during $AgNO_3$ exposure also occurred at the apical membrane (Figure 4B,ii). All considered, these results suggest that differences in the size of the particulates determine the site of Ag deposition, with AgC20 gaining access to the basolateral membrane, while 110 nm particles are confined to the apical membrane. To further explore the idea of AgNP internal localization, TEM and EDS analysis (data not shown) were carried out on tissue sections to try to capture *in situ* localization. However, due to spatiotemporal and sampling difficulties, no ultrastructural evidence of the presence of particles could be obtained.

Na^+/K^+ ATPase Immunohistochemistry Staining and Activity Demonstrate Size-Dependent Effects of Nano-Ag. We were interested in exploring a possible link between Ag deposition in the basolateral membranes of the gills and intestines and any possible effects on the ionoregulatory Na^+/K^+ ATPase channel, which is also found in the basolateral membrane (Figure 5A,i,ii). The Na^+/K^+ ATPase is a known molecular target for Ag^+, which can compete for Na^+ and disrupt the function and integrity of the channel.[21] In the first experiment, we measured the ATPase activity in the homogenates from gill and intestinal tissues collected on day 4. Because ionic Ag has been shown to affect gill ATPase activity,[24] gills collected from $AgNO_3$-treated animals were used as a positive control, which confirmed a 33% decrease in enzyme activity (Figure 5B,i). While both particulates could induce a significant decrease ($p < 0.05$) in ATPase activity in the gill compared with nonexposed animals, AgC20 exposure was associated with a significantly greater reduction (57%) compared with AgC110 (21%). The same trend was observed in the intestines (Figure 5B,ii), where ATPase activity declined to 43% and 54%, respectively, for the ionic control and AgC20. Interestingly, AgC110 had no effect on enzyme activity.

In the second experiment, we determined whether the reduction in ATPase activity is accompanied by structural changes in the ion channels. We used a monoclonal antibody staining of the α-subunit of the ion channel to conduct fluorescence microscopy. As shown in Figure 5A,iii,iv, the exposure to AgC20 was associated with decreased staining intensity of α-subunit in comparison to nonexposed animals. All considered, there was a good agreement between the reduction in Na^+/K^+ ATPase activity and damage to a structural component of the same ion exchange channel. Moreover, these changes are coincident with the site of AgC20 deposition in the basolateral membrane.

DISCUSSION

In this study, we demonstrate size-dependent toxicity of citrate-coated 20 and 110 nm Ag NPs in the gills

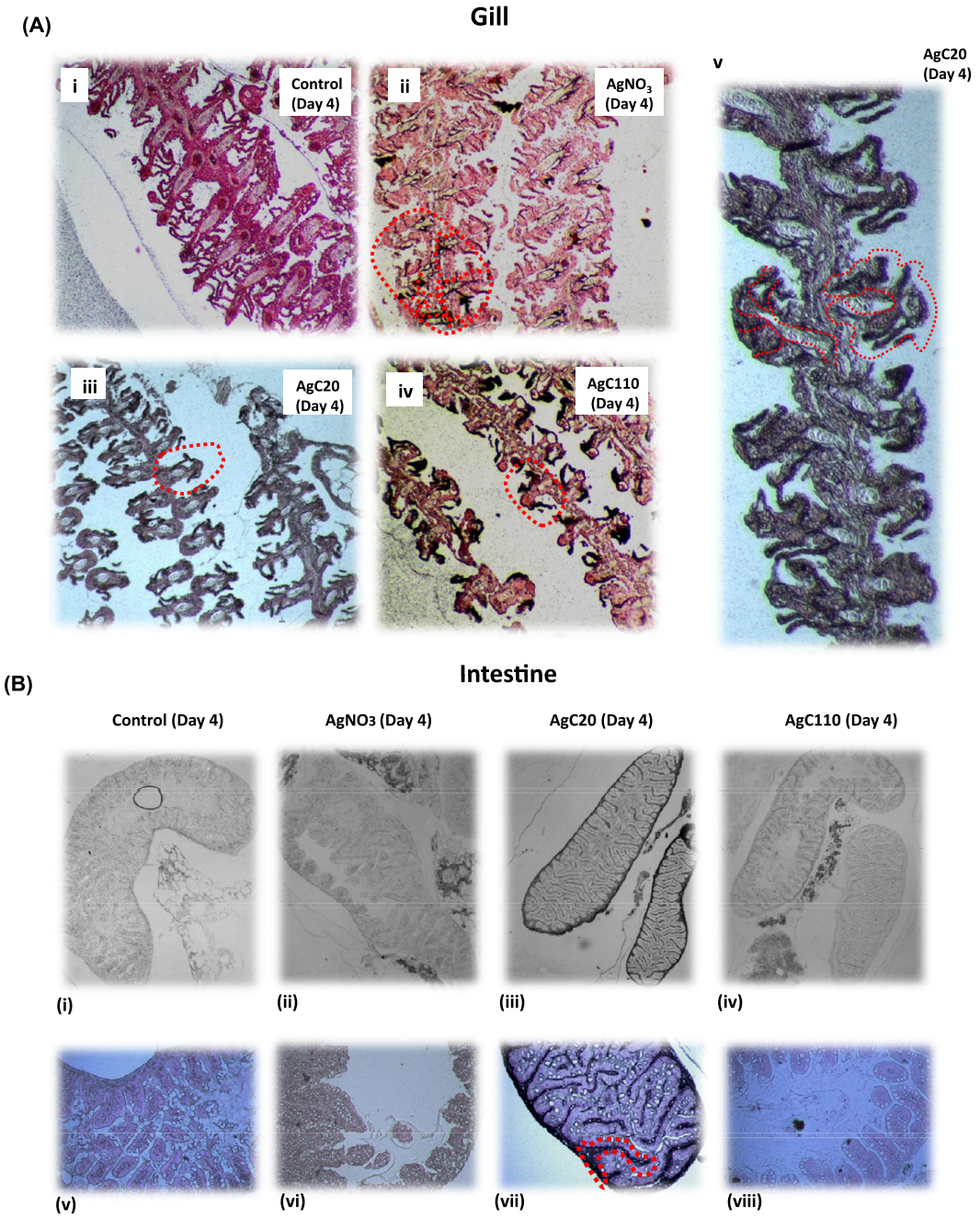

Figure 4. Ag staining of gill and intestinal tissues to demonstrate the sites of Ag deposition. (A) Ag staining of gill tissue, 20× magnification. Please notice that particulate Ag localizes primarily in secondary filaments, while $AgNO_3$ primarily leads to staining in primary filaments. Please also note and refer to the idealized diagrams Figure S2 and S3 in the Supporting Information. (i) Image of a normal gill; (ii) $AgNO_3$ treated fish, with the dotted red line highlighting the Ag in the primary filaments; (iii) AgC20 treated fish, with the dotted line highlighting Ag localization in the secondary filaments; (iv) AgC110 treated fish, with the line highlighting Ag staining of the secondary filaments; (v) close up view from AgC20 treated fish, outlining of Ag staining of primary and secondary filaments. (B) Ag staining of intestinal tissue, 5× magnification. Please notice that AgC20 exposure leads to Ag deposition in the basolateral membranes while AgC110 does not. (i) control image; (ii) $AgNO_3$ treated animals, showing Ag deposition on the apical surface; (iii) AgC20 treated animals, showing prominent staining of the basolateral membrane; (iv) AgC110 animals showing Ag staining at the apical surface. Panels (v−viii) represent 20× magnification: (v) control image; (vi) $AgNO_3$ treated animals; (vii) AgC20 treated animals showing Ag localization the basolateral membranes, outlined by a dotted line; (viii) AgC110 treated animals showing less Ag staining at the apical surface membrane.

and intestines of adult zebrafish. By employing an array of qualitative and quantitative techniques, we demonstrate size-dependent differences in the toxicokinetics, histopathology, and locality of Ag staining, as well as a reduction of ATPase activity in gills and intestines. We also demonstrate Ag bioaccumulation, following a depuration period, in adult zebrafish exposed to nano-Ag but not the ionic form.

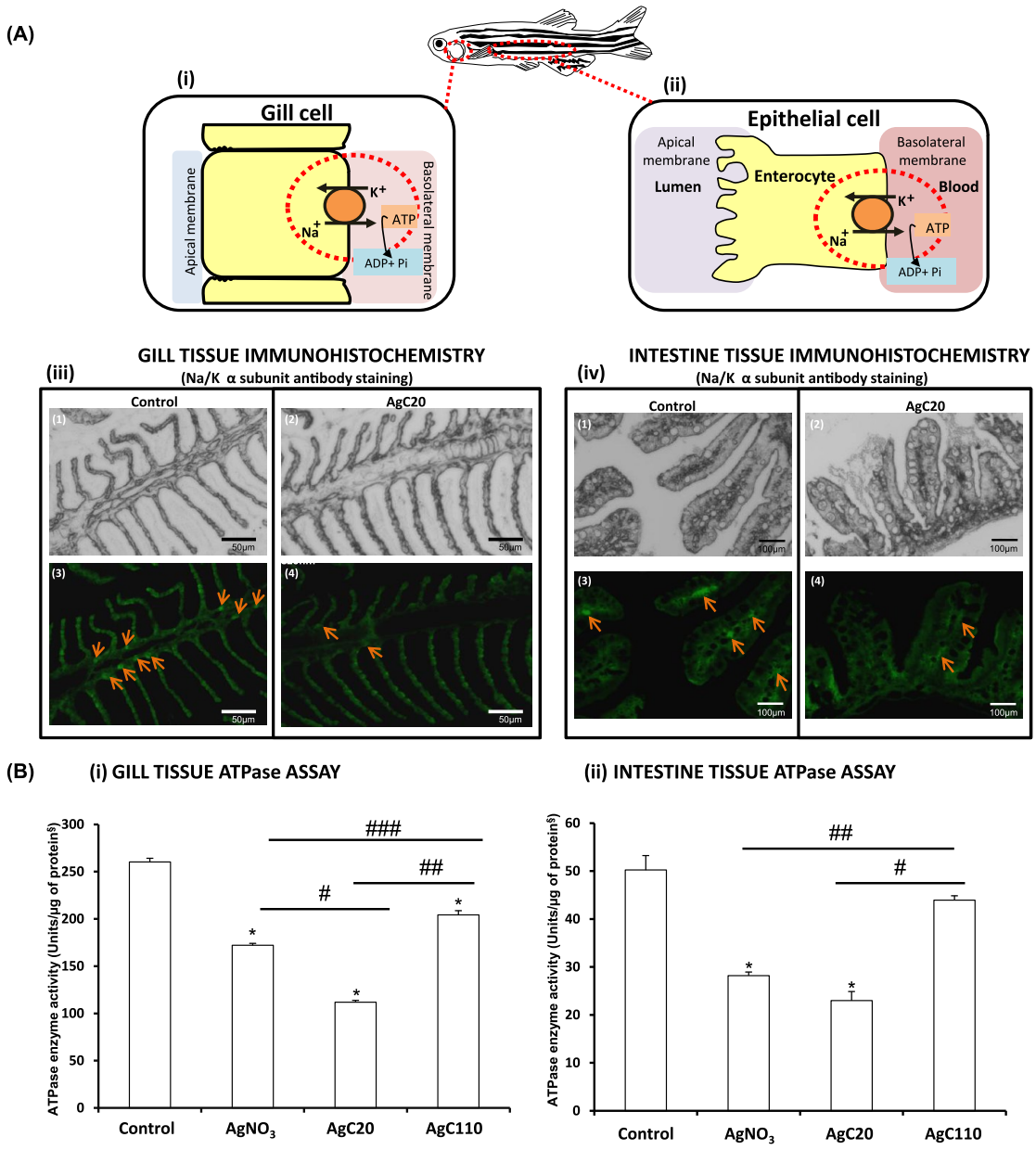

Figure 5. Schematic to explain immunohistochemical staining and assessment of enzymatic activity of the Na^+/K^+ ATPase channel. (A) Schematic diagrams to illustrate the location of the Na^+/K^+ ATPase pump, together with experimental data on the immunohistochemical localization of the α-subunit of the Na^+/K^+ ATPase pump in gill and intestine tissues. (i) Diagram to explain the function and localization of the Na^+/K^+ ATPase pump in the basolateral membrane of the gill; (ii) diagram for enterocytes. Immunohistochemistry staining of the α-subunit of the Na^+/K^+ ATPase in gill (iii) and intestinal (iv) tissues, using FITC staining (α subunits identified by the arrows). The fluorescence images (panels 3 and 4) of controlled and exposed animals are compared with the brightfield images (panels 1 and 2). (B) Graphs depicting relative amounts of ATPase enzymatic activity, expressed as units/μg of protein in the gill (i) and intestinal (ii) tissues following $AgNO_3$, AgC20, and AgC110 exposure. §One unit is the amount of enzyme that catalyzes the production of 1 μmol of free phosphate per minute under the assay conditions. *$p < 0.05$ compared with control group; #, ##, and ### denote $p < 0.05$ between groups.

The most important finding of this study is the striking and consistent size-dependent differences between AgC20 and AgC110 in the zebrafish gills and intestines. ICP-OES analysis of gills demonstrated that AgC20 exposure for 4 h or 4 days resulted in enhanced Ag uptake compared with fish treated with AgC110 or $AgNO_3$ (Figure 2A). We propose that this increased bioavailability is directly related to the smaller size and larger surface area of the small particles, providing increased adherence, penetration, and deposition in primary and secondary gill filaments (Figure S2). These differences were confirmed by Ag staining (Figure 4A,iii). The increased Ag bioavailability in AgC20- compared with AgC110-treated animals also correlates with more severe tissue injury, fusion, and hyperplasia of the gills during histopathological analysis (Figure 3A,iii). These histological changes are commonly seen in the gills of Ag exposed fish.[25] It is also known that gill hyperplasia

in response to other noxious chemicals can enhance xenobiotic uptake in the body of the fish.[26] Further, it has also been established that xenobiotic-induced stress in the fish gill leads to mucus hypersecretion as a protective mechanism.[27] This could create a sticky surface for NPs to adhere to, as seen in other NP studies in fish.[28] Based on the predominant localization of Ag on the secondary filaments in the AgC20 exposed group (Figure 4A,iii), we propose that the accompanying tissue injury and mucus hypersecretion could accentuate the adherence of smaller particles to these filaments; in contrast, there is less impact on primary filaments (Figure 4A,v). We propose that exposure to the ionic form of Ag douses the gill without adhering to the filaments (Figure S2D); this could explain why $AgNO_3$ exposure principally impacts primary rather than secondary filaments (Figure 4A,ii).

The intestines also demonstrated similar but not identical size-dependent effects. There was a striking difference in the localization of AgC20 (Figure 4B,iii) in the basolateral membranes (Figure S3A), compared with the AgC110 distribution at the apical membrane (Figure 4B,iv). There are a number of possible explanations, one of which is that AgC20 particles have higher rates of dissolution in HM (Figures 1B). In particular, we noted that compared with HM, the bathing of 20 nm particles in simulated intestinal fluid resulted in considerable size reduction, whereas for AgC110 particles the size and shape remained approximately the same (Figure S1). Particle size and surface area could be responsible for a larger number of AgC20 particles adhering to the microvilli (Figure S3B). One possibility is that smaller particles could be more rapidly taken up by endocytosis in the epithelial layer,[29] thereby acting as a delivery vehicle for increased Ag deposition in the basolateral membrane of intestinal tissues.[17] Just as in the gill, AgC20 caused more intestinal injury than AgC110. This manifested as an increased number of mucus-secreting goblet cells in the mucosa (Figure 3B,vii; Figure S3A1). Again, the increased secretory response could provide defense against mucosal injury. Interestingly, AgC20 also resulted in a decrease in the abundance of microvilli (Figure 3B,vii), which was not seen for AgC110 (Figure 3B,viii). This loss of microvilli likely reflects local cytotoxicity as a result of a large number of Ag shedding particles adhering to the microvilli (Figure S3B).

The gill is a multifunctional organ that participates in respiration, ionoregulation, acid base regulation and nitrogenous waste excretion in the fish.[30] It has been established that Ag^+ can be mistaken for Na^+ (Figure S4) by the Na^+/K^+ ATPase pump (Figure 5A,i) found in the gill ionocytes.[31] This could lead to a disruption of Na^+/K^+ ATPase activity and the ionoregulatory function of the ion channel.[8] Pump failure is known to lead to disruption of ionic efflux and paracellular leakage, with harmful consequences to the gill.[32] It is therefore noteworthy, that an ATPase assay could confirm that AgC20 has a more severe impact on enzymatic activity than AgC110 or the ionic control (Figure 5B,i). This is also in agreement with a recent study in trout (*Oncorhynchus mykiss*), where it was demonstrated that exposure to citrate-coated AgNPs leads to an inhibition Na^+/K^+ ATPase in the gills.[33] We propose that the AgC20 caused a greater reduction in enzyme activity in the gill because of increased uptake and localized Ag deposition.

The Na^+/K^+ ATPase pump also plays an important role in the basolateral membrane of enterocytes (Figure 5A,ii), where it is important for water and electrolyte balance,[34] as well as contributing to the absorption of nutrients from the food.[35] As for the gill, we demonstrated that AgC20 had a strikingly greater reduction in enzymatic activity than AgC110 (Figure 5B,ii), which had no effect. This novel finding agrees with demonstration of Ag deposition in the basolateral membrane of the intestinal epithelial cells during Ag staining (Figure 4B,vii). It is possible that the generation of inflammation at the same tissue site could contribute to damaging the ATPase, which agrees with studies on human epithelial surfaces, where it has been demonstrated that a reduction in Na^+/K^+ ATPase activity correlates with the presence of inflammation.[36] It is known that reduction in ATPase activity leads to a loss of the ionic gradient, which can lead to structural changes to the cytoskeleton.[37] Thus, the reduced ATPase activity seen during AgC20 exposure could contribute to the structural changes seen in the intestinal lamina propria (Figure 3 B,vi).

We speculate that the main factor contributing to size-dependent differences between nanoparticle sizes is Ag bioavailability. Based on our previous research, we have shown that smaller particles (*e.g.*, AgC20) have higher dissolution rates than larger particles[19] due to their increased surface area. We confirmed that this is true for the particles in this study, as demonstrated by dissolution data showing a higher rate of AgC20 dissolution compared with AgC110 (Figure 1B,ii). Therefore, we surmise that the AgC20 particles are highly efficient carriers for local release and deposition of Ag ions in the fish gill.[17] Consequently, this could result in site-specific disruption of Na^+/K^+ ATPase activity by smaller particles, resulting in more severe local injury and impact on enzymatic activity in the locality of the basolateral membrane (Figure 4B,vi and Figure 2B). Since Na^+/K^+ ATPase activity is also involved in the formation of tight junctions,[38] disintegration of these adhesion sites could allow even more particle entry.[39] Additionally, we also know from one study using frog skin that Ag^+ can induce more Na^+ efflux, causing more permeability[40] and Ag^+ entry into the cell. This provides another possible reason for observing heavy Ag staining in the basolateral membranes of intestines of fish treated with AgC20 (Figure 4B,vii). Moreover, utilizing assays for ATPase

activity (Figure 5B,i,ii) and performance of immunohistochemistry (Figure 5A,iii,iv), we were able to link a mechanistic adverse outcome pathway to the accentuated hazardous potential of AgC20 *in vivo* (Figure 5A, iii,iv). Since the α subunit contains the ATP binding site, we postulate that this enzymatic component plays an important role in the exaggerated effect of AgC20, which partitions more readily to the tissue localization sites of the enzyme.[41]

Interestingly, although the $AgNO_3$ treatment generated more Ag uptake in the intestines (Figure 2B) at 4 h and 4 days, only the nanoparticulate forms were retained post-depuration, highlighting the importance of bioaccumulation in the injurious impact of this metal. Bioaccumulation is a key issue from an environmental perspective because it is essential to detoxify and excrete xenobiotics, in this case Ag, for the organism to survive. This notion is supported by the findings of Jang et al., who demonstrated in a study using carp that Ag retention in the gill and intestine could be observed through to the post-depuration for fish originally exposed to AgNP.[42] Other aquatic organisms such as daphnia also showed Ag accumulation postexposure to citrate coated AgNPs.[43] This bioaccumulation could lead to biomagnification and bioconcentration values, something that was recently investigated using gold NPs.[44] Therefore, contemporary research and the data in this study call for further exploration into bioaccumulation studies.

CONCLUSION

Our study has revealed and elucidated size-dependent differences for 20 and 110 nm particles by adopting a comprehensive *in vivo* approach in adult zebrafish. We established that for the AgC20 particles they exerted a higher Ag uptake, induced greater toxicity on target organs, and caused heavy Ag deposition localization in the basolateral membranes. Moreover, we demonstrate that the *in vivo* effects correlate with a mechanism of action that is traceable to an inhibition of ATPase enzyme activity.

MATERIALS AND METHODS

Ag Nanoparticle Acquisition and Physiochemical Characterization. Two citrate-coated AgNPs with primary sizes 20 and 110 nm (AgC20 and AgC110) were purchased from nanoComposix, San Diego, CA. To determine the primary size/shape of the particles, TEM analysis was performed by placing a drop of the particles, suspended in Holtfreter's medium (HM) or DI water, on a TEM grid, followed by evaporation at room temperature. The images were obtained in a JEOL 1200 EX TEM microscope. The hydrodynamic size and surface charge of the particles, suspended in DI water or HM, were determined using a ZetaPALS instrument (Brookhaven Instrument, Holtsville, NY).

Fish Husbandry. Prior to exposure, wild-type adult zebrafish of the AB strain (6−12 months old) were kept in 6 L tanks in the UCLA zebrafish facility on a 14 h light/10 h dark cycle with a daily water change. Fish were fed artemia twice a day. All procedures were carried out in accordance with the Animal Care and Use Committee guidelines at UCLA.

Experimental Exposure Conditions. Because there is limited data[45] on the amount of AgNPs during aquatic environmental exposures, we do not know what is an environmentally relevant concentration for nano-Ag. Accordingly, the AgNP concentration used in this study (1 ppm) was determined by a dosimetry threshold analysis wherein nano-Ag and $AgNO_3$ were used at 1, 2.5, and 5 ppm, initially, to establish a concentration that does not result in acute developmental or survival effects in fish (Figure S5). A pulse exposure was established to minimize material use and the exposure period (Scheme 1). There were four exposure groups, namely, fish exposed to citrate only (to mimic the effect of the coating material), fish exposed to 20 nm citrate-coated particles (AgC20), fish exposed to 110 nm citrate-coated particles (AgC110), and fish exposed to ionic $AgNO_3$ (with added citrate). Exposures were conducted in 2 L tanks for each group. Each treatment group included 6 male and 6 female fish per exposure. Exposures began on day 1, introducing the equivalent of 1 ppm Ag to each group. AgCNPs were bath-sonicated for 10 min prior to mixing/stirring in each of the 2 L tanks. The fish were then carefully placed into the designated tanks. On the third day of exposure, the fish were fed artemia and the medium was refreshed. After 4 days of exposure, the same fish were transferred into clean medium for a depuration of 7-days. Sacrifice was performed at three time points (Scheme 1), day 1 (after a 4 h of exposure), day 4 (96 h of exposure, but no depuration period), and day 11 (96 h of exposure plus a 7 day depuration period). The experiment was repeated 3 times.

Animal Sacrifice and Biological Sampling. Fish were individually euthanized with Tricaine at the indicated time points (Scheme 1). The target organs, that is, the gills and the intestine, were dissected and either (i) immediately fixed in 4% paraformaldehyde (PFA) for histopathology analysis and immunohistochemistry or (ii) snap frozen for the performance of an ATPase enzymatic assay and ICP-OES analysis. ICP-OES analysis was performed on all the organ samples collected at the times indicated. For histopathology analysis, organs were harvested at 4 days postexposure and on Day 11. For the ATPase enzymatic assay, analysis organs were harvested at 4 days postexposure. It is important to note that the zebrafish was chosen as a representative environmental fish species in this study given its advantages of high versatility, all year round spawning, sequenced genome, and rapid development. We are aware of other environmental fish species frequently used, for example, trout, but we believe by using the zebrafish organism in this investigation we were able to carry out a much more comprehensive study to delineate size dependent toxicity outcome using a variety of techniques. Granted, we are also aware that one of the disadvantages in using adult zebrafish in toxicological studies is the fact that they are small organisms so harvesting some of its organs for analysis can be challenging.

Histolopathological Analysis. Dissected target organs, collected at the second sacrifice (Scheme 1), underwent 24 h fixation in PFA. The fixed organs were embedded in Histogel (Thermo Scientific Richard-Allan Scientific Specimen Processing Gel, HG-4000-012) and placed in Fisherbrand SURE TEK biopsy cassette taped sleeves. The samples were further processed for resin embedding, sagittal sectioning, and hematoxylin and eosin (H&E) staining in the Pathology and Laboratory Medicine Department at UCLA as described previously.[46] High-resolution images (at both 20× and 40×) were obtained using an automated scanning system (Aperio ScanScope AT).

ICP-OES Analysis To Measure Ag Nanoparticle Dissolution and the Ag Content in Target Organs. To determine particle dissolution and Ag release into the suspending medium, particles were suspended at 1 ppm in HM and DI for 4 h or 4 days to reflect the exposure time periods (Scheme 1). After vortexing of the suspensions and centrifugation at 15 000 rpm for 1 h, supernatants were transferred to clean tubes for acid digestion. Digestion was carried out with concentrated nitric acid (10 mL of HNO_3, 65−70%,

Trace Metal grade) at 80 °C for 6 h in a HotBlock (SC100, Environmental Express). The temperature was increased to 95 °C to evaporate the remaining liquid. The samples were cooled at room temperature and resuspended in 2% nitric acid at 80 °C for 3 h to extract analytes. These extracts were transferred to 15 mL ICP-OES analysis tubes and brought to a final volume of 8 mL through the addition of nitric acid. ICP-OES analysis was carried out in a Shimadzu ICPE 9000 to determine the elemental Ag concentration. A calibration curve was established using a standard Ag solution (Elements Inc., 1000 mg/L in 2% HNO_3). Each sample and standard was analyzed in triplicate in the presence of 2% (v/v) nitric acid. To determine the Ag content of the gills and intestines, ICP-OES analysis was performed on the target organs as described above. The same procedure was followed to assess the tissue Ag content. Twelve dissected target organs, that is, gill and intestine, were used for each time point. Ag content was expressed as micrograms of Ag per unitary target organ per adult fish.

Localization of Ag Distribution in the Gill and Intestine using Ag Staining. In order to determine the localization of Ag in the gill and intestine tissues, the paraffin embedded sections for histopathological analysis were sectioned and fixed on Fisherbrand Superfrost Plus slides. The slides with the embedded gill and intestinal tissues were dewaxed with xylene and then rehydrated in a graded ethanol series. The slides were stained using a Silver Enhancing Kit (Ted Pella Inc. Redding. CA), followed by counter staining with Nuclear Fast Red (Vector Laboratories, Inc. Burlingame, CA) according to our previous published protocol.[19]

Assessment of ATPase Enzyme Activity. Snap frozen gill and intestinal tissue, collected at the second sacrifice, were manually homogenized in 400 μL of Tris buffer for 2 min in 1.5 mL Eppendorf tubes. Samples were centrifuged for 5 min at 1400 rpm, and supernatants were transferred to fresh Eppendorf tubes. ATPase enzymatic activity was assessed using the Sigma ATPase kit (MK113), according to manufacturer's instructions. Concentrations were expressed as units per microgram of protein (one unit represents the amount of enzyme producing 1 μmol of free phosphate per minute).

Immunohistochemical Staining for the α Subunit of Na^+/K^+ ATPase. The paraffin embedded sections of harvested organs used (2nd sacrifice, Scheme 1) were sectioned and fixed on Fisherbrand Superfrost Plus slides. Subsequently, the tissues were dewaxed with xylene and then dehydrated by a graded ethanol series. The sections were overlaid with a commercial mouse monoclonal primary antibody, recognizing the α subunit of the Na^+/K^+ ATPase (H3, sc-48345, Santa Cruz Biotechnology). After washing, the slides were overlaid with a fluorescent secondary antibody (IgG_{2b}), followed by reading under the GFP channel (509 nm) in a Zeiss Observer D1 microscope.

Statistical Analysis. Results were analyzed using the two-side Student's *t* test. Differences were regarded as statistically significant when $p < 0.05$. Data were reported as the mean (standard error bars from at least three separate experiments).

Conflict of Interest: The authors declare no competing financial interest.

Acknowledgment. This work is supported by funding from the National Science Foundation and the Environmental Protection Agency under Cooperative Agreement Number DBI 1266377 to UC CEIN. Any opinions, findings, and conclusions or recommendations expressed in this material are those of the author(s) and do not necessarily reflect the views of the National Science Foundation or the Environmental Protection Agency. This work has not been subjected to EPA review, and no official endorsement should be inferred. We acknowledge Linda Dong, Department of Molecular, Cell, and Developmental Biology, University of California, Los Angeles, for the support on zebrafish care and spawning.

Supporting Information Available: The Supporting Information is available free of charge on the ACS Publications website at DOI: 10.1021/acsnano.5b04583.

Additional information on current market products containing AgNPs, representative TEM images of AgNPs in simulated intestinal fluid, idealized diagrams showing the structures of zebrafish gill and intestine, and diagram of Na^+/K^+ ATPase pump (PDF)

REFERENCES AND NOTES

1. Nanowerk. http://www.nanowerk.com/nanomaterial-database.php. Accessed online on March 2015.
2. Woodrow Database. http://www.nanotechproject.org/cpi/ Accessed online on March 2015.
3. Rai, M.; Yadav, A.; Gade, A. Silver Nanoparticles as a New Generation of Antimicrobials. *Biotechnol. Adv.* **2009**, *27*, 76–83.
4. Ahamed, M.; AlSalhi, M. S.; Siddiqui, M. Silver Nanoparticle Applications and Human Health. *Clin. Chim. Acta* **2010**, *411*, 1841–1848.
5. Keller, A. A.; McFerran, S.; Lazareva, A.; Suh, S. Global Life Cycle Releases of Engineered Nanomaterials. *J. Nanopart. Res.* **2013**, *15*, 1692.
6. Gottschalk, F.; Sonderer, T.; Scholz, R. W.; Nowack, B. Modeled Environmental Concentrations of Engineered Nanomaterials (TiO_2, ZnO, Ag, CNT, fullerenes) for Different Regions. *Environ. Sci. Technol.* **2009**, *43*, 9216–9222.
7. Griffitt, R. J.; Luo, J.; Gao, J.; Bonzongo, J. C.; Barber, D. S. Effects of Particle Composition and Species on Toxicity of Metallic Nanomaterials in Aquatic Organisms. *Environ. Toxicol. Chem.* **2008**, *27*, 1972–1978.
8. Webb, N. A.; Wood, C. M. Physiological Analysis of the Stress Response Associated with Acute Silver Nitrate Exposure in Freshwater Rainbow Trout (*Oncorhynchus mykiss*). *Environ. Toxicol. Chem.* **1998**, *17*, 579–588.
9. Allee, W.; Bowen, E. S. Studies in Animal Aggregations: Mass Protection Against Colloidal Silver among Goldfishes. *J. Exp. Zool.* **1932**, *61*, 185–207.
10. Navarro, E.; Piccapietra, F.; Wagner, B.; Marconi, F.; Kaegi, R.; Odzak, N.; Sigg, L.; Behra, R. Toxicity of Silver Nanoparticles to *Chlamydomonas reinhardtii*. *Environ. Sci. Technol.* **2008**, *42*, 8959–8964.
11. Zhao, C. M.; Wang, W. X. Comparison of Acute and Chronic Toxicity of Silver Nanoparticles and Silver Nitrate to *Daphnia magna*. *Environ. Toxicol. Chem.* **2011**, *30*, 885–892.
12. George, S.; Lin, S.; Ji, Z.; Thomas, C. R.; Li, L.; Mecklenburg, M.; Meng, H.; Wang, X.; Zhang, H.; Xia, T.; et al. Surface Defects on Plate-shaped Silver Nanoparticles Contribute to Its Hazard Potential in a Fish Gill Cell Line and Zebrafish Embryos. *ACS Nano* **2012**, *6*, 3745–3759.
13. Bilberg, K.; Malte, H.; Wang, T.; Baatrup, E. Silver Nanoparticles and Silver Nitrate Cause Respiratory Stress in Eurasian perch (*Perca fluviatilis*). *Aquat. Toxicol.* **2010**, *96*, 159–165.
14. Choi, J. E.; Kim, S.; Ahn, J. H.; Youn, P.; Kang, J. S.; Park, K.; Yi, J.; Ryu, D. Y. Induction of Oxidative Stress and Apoptosis by Silver Nanoparticles in the Liver of Adult Zebrafish. *Aquat. Toxicol.* **2010**, *100*, 151–159.
15. Wu, Y.; Zhou, Q.; Li, H.; Liu, W.; Wang, T.; Jiang, G. Effects of Silver Nanoparticles on the Development and Histopathology Biomarkers of Japanese medaka (*Oryzias latipes*) using the Partial-life Test. *Aquat. Toxicol.* **2010**, *100*, 160–167.
16. Wise, J. P., Sr.; Goodale, B. C.; Wise, S. S.; Craig, G. A.; Pongan, A. F.; Walter, R. B.; Thompson, W. D.; Ng, A. K.; Abouelssa, A.-M.; Mitani, H. Silver Nanospheres are Cytotoxic and Genotoxic to Fish Cells. *Aquat. Toxicol.* **2010**, *97*, 34–41.
17. Shaw, B. J.; Handy, R. D. Physiological Effects of Nanoparticles on Fish: A Comparison of Nanometals *versus* Metal Ions. *Environ. Int.* **2011**, *37*, 1083–1097.
18. Osborne, O. J.; Johnston, B. D.; Moger, J.; Balousha, M.; Lead, J. R.; Kudoh, T.; Tyler, C. R. Effects of Particle Size and Coating on Nanoscale Ag and TiO_2 Exposure in Zebrafish (*Danio rerio*) Embryos. *Nanotoxicology* **2013**, *7*, 1315–1324.
19. Wang, X.; Ji, Z.; Chang, C. H.; Zhang, H.; Wang, M.; Liao, Y. P.; Lin, S.; Meng, H.; Li, R.; Sun, B.; et al. Use of Coated Silver Nanoparticles to Understand the Relationship of Particle Dissolution and Bioavailability to Cell and Lung Toxicological Potential. *Small* **2014**, *10*, 385–398.

20. Wood, C. M.; Hogstrand, C.; Galvez, F.; Munger, R. The Physiology of Waterborne Silver Toxicity in Freshwater Rainbow Trout (*Oncorhynchus mykiss*) 1. The Effects of Ionic Ag^{+}. *Aquat. Toxicol.* **1996**, *35*, 93–109.
21. Wood, C. M.; Playle, R. C.; Hogstrand, C. Physiology and Modeling of Mechanisms of Silver Uptake and Toxicity in Fish. *Environ. Toxicol. Chem.* **1999**, *18*, 71–83.
22. Bianchini, A.; Wood, C. M. Physiological Effects of Chronic Silver Exposure in *Daphnia magna*. *Comp. Biochem. Physiol., Part C: Toxicol. Pharmacol.* **2002**, *133*, 137–145.
23. Griffitt, R. J.; Hyndman, K.; Denslow, N. D.; Barber, D. S. Comparison of Molecular and Histological Changes in Zebrafish Gills Exposed to Metallic Nanoparticles. *Toxicol. Sci.* **2009**, *107*, 404–415.
24. Bury, N.; Grosell, M.; Grover, A.; Wood, C. ATP-dependent Silver Transport across the Basolateral Membrane of Rainbow Trout Gills. *Toxicol. Appl. Pharmacol.* **1999**, *159*, 1–8.
25. Johari, S. A.; Kalbassi, M. R.; Yu, I. J.; Lee, J. H. Chronic Effect of Waterborne Silver Nanoparticles on Rainbow Trout (*Oncorhynchus mykiss*): Histopathology and Bioaccumulation. *Comp. Clin. Pathol.* **2014**, 10.1007/s00580-014-2019-2.
26. Spry, D. J.; Wood, C. M. Zinc Influx Across the Isolated, Perfused Head Preparation of the Rainbow Trout (*Salmo gairdneri*) in Hard and Soft Water. *Can. J. Fish. Aquat. Sci.* **1988**, *45*, 2206–2215.
27. Bonga, S. W. The Stress Response in Fish. *Physiol. Rev.* **1997**, *77*, 591–625.
28. Smith, C. J.; Shaw, B. J.; Handy, R. D. Toxicity of Single Walled Carbon Nanotubes to Rainbow Trout,(*Oncorhynchus mykiss*): Respiratory Toxicity, Organ Pathologies, and other Physiological Effects. *Aquat. Toxicol.* **2007**, *82*, 94–109.
29. Kettler, K.; Veltman, K.; van de Meent, D.; van Wezel, A.; Hendriks, A. J. Cellular Uptake of Nanoparticles as Determined by Particle Properties, Experimental Conditions, and Cell Type. *Environ. Toxicol. Chem.* **2014**, *33*, 481–492.
30. Wood, C. M. Toxic responses of the gill. In *Target Organ Toxicity in Marine and Freshwater Teleosts*; Taylor and Francis: London, 2001; pp 1−89.
31. Klyce, S. D.; Marshall, W. S. Effects of Ag^{+} on Ion Transport by the Corneal Epithelium of the Rabbit. *J. Membr. Biol.* **1982**, *66*, 133–144.
32. Evans, D. H. The Fish Gill: Site of Action and Model for Toxic Effects of Environmental Pollutants. *Environ. Health Persp.* **1987**, *71*, 47.
33. Schultz, A. G.; Ong, K. J.; MacCormack, T.; Ma, G.; Veinot, J. G.; Goss, G. G. Silver Nanoparticles Inhibit Sodium Uptake in Juvenile Rainbow trout (*Oncorhynchus mykiss*). *Environ. Sci. Technol.* **2012**, *46*, 10295–10301.
34. Loretz, C. A. Electrophysiology of Ion Transport in Teleost Intestinal Cells. In *Cellular and Molecular Approaches to Fish Ionic Regulation*; Wood, C. M., Shuttleworth, T. J., Eds.; Academic Press: San Diego, CA, 1995; pp 25−56.
35. Buddington, R. K.; Krogdahl, A.; Bakke-McKellep, A. M. The Intestines of Carnivorous Fish: Structure and Functions and the Relations with Diet. *Acta Physiol. Scand.* **1997**, *638*, 67–80.
36. Allgayer, H.; Kruis, W.; Paumgartner, G.; Wiebecke, B.; Brown, L.; Erdmann, E. Inverse Relationship between Colonic (Na^{+} K^{+})-ATPase Activity and Degree of Mucosal Inflammation in Inflammatory Bowel Disease. *Dig. Dis. Sci.* **1988**, *33*, 417–422.
37. Lopina, O. Na^{+}, K^{+}-ATPase: Structure, Mechanism, and Regulation. *Membr. Cell. Biol.* **1999**, *13*, 721–744.
38. Rajasekaran, A. K.; Rajasekaran, S. A. Role of Na-K-ATPase in the Assembly of Tight Junctions. *AM J. Physiol-Renal.* **2003**, *285*, F388–F396.
39. Fromter, E.; Diamond, J. Route of Passive Ion Permeation in Epithelia. *Nature. New. Biol.* **1972**, *235*, 9–13.
40. Curran, P. F. Effect of Silver Ion on Permeability Properties of Frog Skin. *Biochim. Biophys. Acta, Biomembr.* **1972**, *288*, 90–97.
41. Lingrel, J. B.; Kuntzweiler, T. Na^{+}, K^{+}-ATPase. *J. Biol. Chem.* **1994**, *269*, 19659–19662.
42. Jang, M.-H.; Kim, W.-K.; Lee, S.-K.; Henry, T. B.; Park, J. W. Uptake, Tissue Distribution, and Depuration of Total Silver in Common Carp (*Cyprinus carpio*) after Aqueous Exposure to Silver Nanoparticles. *Environ. Sci. Technol.* **2014**, *48*, 11568–11574.
43. Khan, F. R.; Paul, K. B.; Dybowska, A. D.; Valsami-Jones, E.; Lead, J. R.; Stone, V.; Fernandes, T. F. Accumulation Dynamics and Acute Toxicity of Silver Nanoparticles to *Daphnia magna* and *Lumbriculus variegatus*: Implications for Metal Modeling Approaches. *Environ. Sci. Technol.* **2015**, *49*, 4389–4397.
44. Judy, J. D.; Unrine, J. M.; Bertsch, P. M. Evidence for Biomagnification of Gold Nanoparticles within a Terrestrial Food Chain. *Environ. Sci. Technol.* **2011**, *45*, 776–781.
45. Sun, T. Y.; Gottschalk, F.; Hungerbühler, K.; Nowack, B. Comprehensive Probabilistic Modelling of Environmental Emissions of Engineered Nanomaterials. *Environ. Pollut.* **2014**, *185*, 69–76.
46. Lin, S.; Wang, X.; Ji, Z.; Chang, C. H.; Dong, Y.; Meng, H.; Liao, Y.-P.; Wang, M.; Song, T. B.; Kohan, S.; et al. Aspect Ratio Plays a Role in the Hazard Potential of CeO_2 Nanoparticles in Mouse Lung and Zebrafish Gastrointestinal Tract. *ACS Nano* **2014**, *8*, 4450–4464.